Proximity effects in superconducting spin-valve structures
Flokstra, M.G.

Chapter 7

Critical voltage of a mesoscopic superconductor

7.1   Introduction

The energy distribution function of quasiparticles in a normal metal is under equilibrium conditions given by the Fermi-Dirac distribution $f_{\mathrm{FD}} = \frac{1}{e^{(\beta\varepsilon)}+1}$ with $\beta \equiv 1/(k_BT)$ and ε the energy of the quasiparticle measured with respect to the Fermi energy. In recent years it has been demonstrated that in a voltage (V)-biased mesoscopic wire (length L) a two-step non-equilibrium distribution develops [78] with additional rounding by quasiparticle scattering due to spin-flip and/or Coulomb interactions [79]. Figure 7.1a shows the distribution, which resembles two shifted Fermi-Dirac functions:

$$f(x, \varepsilon) = (1 - x) f_{\mathrm{FD}}(\varepsilon + eV/2) + x f_{\mathrm{FD}}(\varepsilon - eV/2) \qquad (7.1)$$

with x the coordinate along the wire. For strong enough relaxation ($L \gg L_\phi$, with L_ϕ the phase coherence length) and/or high temperatures ($k_BT \gg eV$) the distribution returns to a Fermi-Dirac distribution with a local effective temperature.
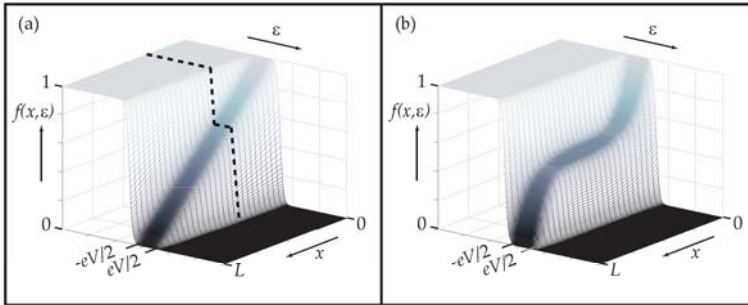

Figure 7.1: Quasiparticle distribution function $f(x, \varepsilon)$ as function of energy ε and position x for a normal wire (a) and a superconducting wire (b) between normal metallic reservoirs for $k_BT \ll eV < \Delta_0$. The dashed line showing the two-step distribution at a fixed location along the wire.

If the normal wire is replaced by a superconducting wire, the attractive interaction between electrons leads to the superconducting state. The questions we address here are how the distribution function inside the superconducting wire is modified (for a typical result see Fig. 7.1b) and how this affects observable properties such as the current-voltage characteristics of the system and the breakdown of the superconducting state. To relate the distribution function to observable quantities, it is convenient to separate the symmetric part f_L (energy mode) from the asymmetric part f_T (charge mode). Here, the
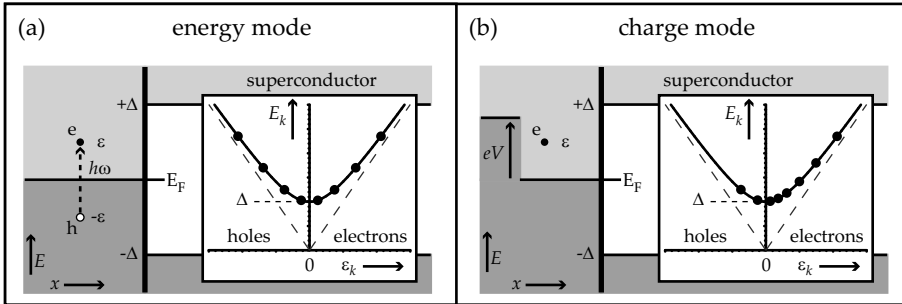
Figure 7.2: An electron excitation in a normal metal created by (a) radiation (of energy $h\omega$) and (b) a potential difference eV (from a connecting reservoir). The excitation in (a) is symmetric in terms of electrons and holes and contributes to the energy mode. The excitation in (b) is antisymmetric and contributes to the charge mode. The insets in both graphs show how these two modes occupy states in the excitation energy spectrum E_k of the superconductor. Here, $E_k = \sqrt{\Delta^2 + \varepsilon_k^2}$ where Δ is the gap energy and ε_k the energy of the single electron state with wave vector $\mathbf{k}$.

symmetry is in terms of electrons versus holes. In a normal metal, an electron that is excited above the Fermi level at energy ε leaves a hole below the Fermi level at energy $-\varepsilon$. This contributes to the energy mode, and common sources for such symmetric excitations are temperature and radiation (see Fig. 7.2a). The charge mode is asymmetric in electrons and holes. It counts the number of excess electrons or holes in the system. Such asymmetric excitations are created by electrical potential differences (see Fig. 7.2b). The energy mode and charge mode each have a different spatial and spectral form. The decomposition of the typical result shown in Fig. 7.1b into the energy mode and charge mode is shown in Fig. 7.3. The exchange of electrons between the normal metal (reservoir) and the superconducting wire is for sub-gap energies controlled by the Andreev reflection process. The question we thus address is how f_L and f_T enter/behave in the superconductor, and how that changes its transport properties. In particular, we investigate how the breakdown of the superconducting state occurs.

The transport and spectral properties of dirty superconducting systems ($\ell_e \ll \xi_0$, with ℓ_e the elastic mean free path and ξ_0 the superconducting phase coherence length) are described by the quasiclassical Green functions obeying the Usadel equation [19]. For out of equilibrium systems we use the Keldysh technique in Nambu (particle-hole) space, neglecting spin dependent interactions and assuming conventional superconductivity. Furthermore, we ignore inelastic scattering in the wire and use the time independent formalism. We assume this to be an acceptable simplification at temperatures far below
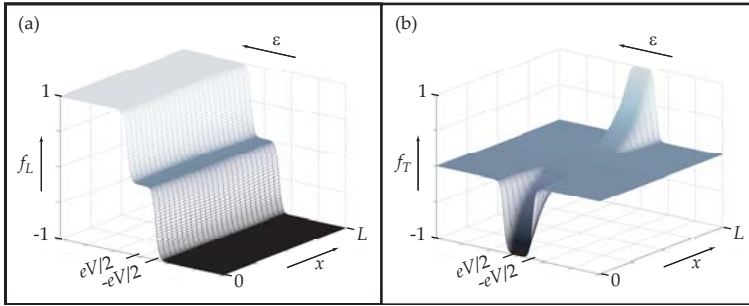
Figure 7.3: Decomposition of the quasiparticle distribution function $f(x,\varepsilon)$ as shown in Fig. 7.1b into the energy mode f_L and charge mode f_T.

the critical temperature T_c, and for large enough wire cross section. In this way the role of thermally activated and respectively quantum phase slips is ruled out [80, 81].

7.1.1   Usadel equation using Keldysh technique

The Keldysh technique is based upon a special ordering of the Green functions, and the main result is that the Green functions are split into three parts. The retarded $\left(\check{G}^R\right)$ and advanced $\left(\check{G}^A\right)$ parts describe the propagation of particles (electrons and holes) in respectively positive and negative time direction, while the Keldysh $\left(\check{G}^K\right)$ part describes the non-equilibrium part of the system. As long as a system is in equilibrium (i.e the quasiparticles are distributed like a Fermi-Dirac distribution with an effective temperature), it is fully characterized by the retarded Green functions, and we can calculate the density of states, electrical current, etc. with the knowledge of the retarded Green functions alone. This changes when the system is driven out of equilibrium, for then we also need to know which energy states are accessible. In other words, we need to know the non-equilibrium distribution function of the quasiparticles. In that case we need to solve the Keldysh Green functions, for which in turn we need both the retarded and advanced Green functions. The latter is actually only necessary when the time symmetry of the system is broken, for example, due to magnetic fields. Otherwise, it follows straightforwardly from the retarded Green functions. Each of these three parts are Nambu⊗spin space matrices (for their elements see Eq. 2.9 - 2.10), and can be collected together into the Keldysh space effectively creating a matrix Green function of dimension 8×8. This new matrix Green function then replaces the matrix Green function in the Usadel equation, and the remaining Nambu⊗spin space

matrices of the Usadel equation are projected onto the 2×2 unity matrix $\hat{1}$ in Keldysh space. However, in the absence of spin dependent interactions the spin space effectively drops out of the equation and the retarded, advanced, and Keldysh matrix Green function reduce to 2×2 matrices in Nambu space (denoted by a hat). The time independent Usadel equation for an s-wave superconductor (see Eq. 2.20) using the Keldysh technique then takes the form:

$$\hbar D \nabla \left(\check{G} \nabla \check{G} \right) = -i \left[\check{H}, \check{G} \right] \tag{7.2}$$

where D is the diffusion constant and ∇ is the spatial derivative [82]. Furthermore, the spin-flip part vanished because we ignore spin-flip processes in the wire. The elements of $\check{G}$ and $\check{H}$ are 2×2 matrices in Nambu space:

$$\check{G} = \begin{pmatrix} \hat{G}^R & \hat{G}^K \\ 0 & \hat{G}^A \end{pmatrix}, \check{H} = \begin{pmatrix} \hat{H} & 0 \\ 0 & \hat{H} \end{pmatrix} \text{ with } \hat{H} = \begin{pmatrix} \varepsilon & -\Delta \\ \Delta^* & -\varepsilon \end{pmatrix} \tag{7.3}$$

where the chosen gauge is such that the pair potential Δ is in equilibrium a real quantity, $\Delta = \Delta^*$. Inserting these Keldysh space matrices into the Usadel equation results in three equation:

$$\hbar D \nabla (\hat{G}^R \nabla \hat{G}^R) = -i \left[\hat{H}, \hat{G}^R \right]$$

$$\hbar D \nabla (\hat{G}^A \nabla \hat{G}^A) = -i \left[\hat{H}, \hat{G}^A \right] \tag{7.4}$$

$$\hbar D \nabla (\hat{G}^R \nabla \hat{G}^K + \hat{G}^K \nabla \hat{G}^A) = -i \left[\hat{H}, \hat{G}^K \right]$$

The first two equations are the retarded and advanced part of the Usadel equation. The third equation is the kinetic part of the Usadel equation, describing the non-equilibrium. The retarded, advanced and Keldysh matrix Green functions are connected to each other by the normalization condition for the matrix Green function in the Keldysh space: $\check{G}^2 = \check{1}$. Apart from this condition, there is also a direct connection between the retarded and advanced matrix Green function, which differ only in the time direction of the propagation of the particles. In the absence of time symmetry breaking, the two are related through:

$$\hat{G}^A = -\tau_3 \left(\hat{G}^R \right)^\dagger \tau_3 \tag{7.5}$$

and thus finding the retarded Green functions is sufficient to know the advanced Green functions as well. From the normalization condition for $\check{G}$ one obtains $\hat{G}^R \hat{G}^R = \hat{G}^A \hat{G}^A = \hat{1}$ and $\hat{G}^R \hat{G}^K + \hat{G}^K \hat{G}^A = \hat{0}$. These two conditions make that $\hat{G}^K$ can be parameterized as:

$$\hat{G}^K = \hat{G}^R \hat{f} - \hat{f} \hat{G}^A \tag{7.6}$$

It was shown by Schmid and Schön [83], and Larkin and Ovchinnikov [84] that $\hat{f}$ can be chosen as the diagonal generalized distribution number matrix of the quasiparticles in Nambu space: $\hat{f} = f_L(x,\varepsilon)\,\tau_0 + f_T(x,\varepsilon)\,\tau_3$, with f_L the symmetric part (energy mode) and f_T the antisymmetric part (charge mode) of the quasiparticle distribution function. The full distribution function is retained by: $2f(x,\varepsilon) = 1 - f_L(x,\varepsilon) - f_T(x,\varepsilon)$. For a bulk superconductor in equilibrium, this distribution function equals the Fermi-Dirac distribution: $f(x,\varepsilon) = f_{\text{FD}}(x,\varepsilon)$

7.1.2   Working out the equations

The retarded matrix Green function in terms of the position and energy dependent normal $g(\varepsilon,x)$ and anomalous $F_i(\varepsilon,x)$ Green functions is (see Eq. 2.21):

$$\hat{G}^R = \begin{pmatrix} g(\varepsilon,x) & F_1(\varepsilon,x) \\ F_2(\varepsilon,x) & -g(\varepsilon,x) \end{pmatrix} \tag{7.7}$$

where it was used that $\overline{g} = -g$, which one obtains from the normalization condition $\hat{G}^R\hat{G}^R = \hat{1}$. The normalization condition also leads to $g^2 + F_1 F_2 = 1$. Substituting all this in the retarded part of the Usadel equation: $\hbar D\nabla(\hat{G}^R\nabla\hat{G}^R) = -i\left[\hat{H}, \hat{G}^R\right]$, we find the retarded Usadel equations:

$$\begin{aligned} \hbar D\left[g\nabla^2 F_1 - F_1\nabla^2 g\right] &= -2i\Delta g - 2i\varepsilon F_1 \\ \hbar D\left[F_1\nabla^2 F_2 - F_2\nabla^2 F_1\right] &= 2i\Delta F_2 + 2i\Delta^* F_1 \end{aligned} \tag{7.8}$$

The second equation is essential when calculating the non-equilibrium properties of superconductors. Its left-hand-side is proportional to the divergence of the spectral (energy-dependent) supercurrent, which is (compared to the equilibrium case) no longer a conserved quantity.

Using the general relation between the advanced matrix Green function and the retarded matrix Green function: $\hat{G}^R = -\tau_3\left(\hat{G}^A\right)^\dagger \tau_3$, the Keldysh matrix Green function $\hat{G}^K$ can be written entirely in terms of g, F_1, F_2, f_L and f_T:

$$\hat{G}^K = \begin{pmatrix} (g+g^\dagger)f_+ & F_1 f_- - F_2^\dagger f_+ \\ F_2 f_+ - F_1^\dagger f_- & -(g+g^\dagger)f_- \end{pmatrix} \tag{7.9}$$

where $f_\pm = f_L \pm f_T$. Working out the kinetic part of the Usadel equation: $\hbar D\nabla(\hat{G}^R\nabla\hat{G}^K + \hat{G}^K\nabla\hat{G}^A) = -i\left(\hat{H}, \hat{G}^K\right)$ we find (combining the diagonal

components) the kinetic equations describing the non-equilibrium part:

$$\begin{aligned} \hbar D \nabla j_{\text{energy}} &= 0 \\ \hbar D \nabla j_{\text{charge}} &= 2 R_L f_L + 2 R_T f_T \end{aligned} \tag{7.10}$$

The various elements in Eq. 7.10 are given by:

$$\begin{aligned} j_{\text{energy}} &= \Pi_L \nabla f_L + \Pi_X \nabla f_T + j_\varepsilon f_T \\ j_{\text{charge}} &= \Pi_T \nabla f_T - \Pi_X \nabla f_L + j_\varepsilon f_L \\ \Pi_L &= \tfrac{1}{4} \left(2 + 2 |g|^2 - |F_1|^2 - |F_2|^2 \right) \\ \Pi_T &= \tfrac{1}{4} \left(2 + 2 |g|^2 + |F_1|^2 + |F_2|^2 \right) \\ \Pi_X &= \tfrac{1}{4} \left(|F_1|^2 - |F_2|^2 \right) \\ j_\varepsilon &= \tfrac{1}{2} \Re \left\{ F_1 \nabla F_2 - F_2 \nabla F_1 \right\} \\ R_L &= -\tfrac{1}{2} \Im \left\{ \Delta F_2 + \Delta F_1^\dagger \right\} \\ R_T &= -\tfrac{1}{2} \Im \left\{ \Delta F_2 - \Delta F_1^\dagger \right\} \end{aligned} \tag{7.11}$$

Equations 7.10 are two coupled diffusion equations for f_L and f_T, describing the divergences in the spectral energy current and the spectral charge current. The total charge current is given by $J = \frac{1}{2e\rho} \int j_{\text{charge}} d\varepsilon$ with ρ the resistivity. The terms Π_L and Π_T can be related to an effective diffusion constant for the energy and charge mode respectively and Π_X as a "cross-diffusion" between them. j_ε is the spectral supercurrent and R_L and R_T describe the "leakage" of spectral current to different energies, where the total leakage-current $\propto \int (R_L f_L + R_T f_T) d\varepsilon$ is zero. In the small signal limit the terms Π_X, j_ε and R_L are small and can in many cases be neglected (linear approach), effectively decoupling f_L and f_T. In this work, we go beyond this limit. The Usadel equation is supplemented by a self-consistency relation:

$$\hat{H}_{(1,2)} = \frac{N_0 V_{\text{eff}}}{4} \int_{-\hbar\omega_D}^{\hbar\omega_D} \hat{G}_{(1,2)}^K d\varepsilon \tag{7.12}$$

Here, N_0 is the normal density of states around the Fermi energy, V_{eff} the effective attractive interaction and the integral limits are set by the Debye energy $\hbar\omega_D$. The resulting equation for Δ becomes:

$$\Delta = -\frac{1}{4} N_0 V_{\text{eff}} \int_{-\hbar\omega_D}^{\hbar\omega_D} \left((F_1 - F_2^\dagger) f_L - (F_1 + F_2^\dagger) f_T \right) d\varepsilon. \tag{7.13}$$

To calculate spectral and transport properties, one needs to know the self-consistent solution of Δ. In most practical cases, this has to be done numerically. A convenient solution scheme is to first find the Green functions of the system by solving the retarded equations for a certain Δ, next to determine the quasiparticle distribution functions by solving the kinetic equations and then calculate a new Δ using the self-consistency relation. This process has to be repeated until Δ converges. As a starting value for Δ we use the BCS form at zero temperature. A typical solution employs a grid of in the order of 10^4 energies, 10^2 spatial coordinates, and 10^3 iterations of Δ. The stability of the solution scheme was tested extensively by inserting different initial values. At all the applied voltages self-consistent steady state solutions are found. To simplify the calculations a parameterization is used that automatically fulfills the normalization condition. It is convenient to take $g = \cosh(\theta)$, $F_1 = \sinh(\theta)e^{i\chi}$ and $F_2 = -\sinh(\theta)e^{-i\chi}$, where θ and χ are position and energy dependent (complex) variables. At the interfaces between the superconducting wire and the normal metallic reservoirs we use the following boundary conditions: $\theta = \nabla\chi = 0$ (retarded equation) and $f_{L,T} = \frac{1}{2}(\tanh\frac{\varepsilon+eV}{2k_BT} \pm \tanh\frac{\varepsilon-eV}{2k_BT})$ (kinetic equation), where the latter are the usual reservoir distribution functions.

7.1.3   Simulation on the NSN system

The transport properties of the NSN system (see Inset Fig. 7.4) can now be calculated with the equations described above. In a previous analysis a finite differential conductance was found at zero bias employing a linear response calculation [85]. With the approach introduced here, the full current-voltage relation can be obtained. The result at several temperatures is displayed in Fig. 7.4, with the voltage normalized to $\Delta_0(= \Delta_{\text{bulk},T=0})$ and the current density normalized to the critical current density $J_c \approx 0.75\frac{\Delta_0}{\xi_0\rho e}$ [86], with $\xi_0 = \sqrt{\hbar D/\Delta_0}$. At $T = 0$ we observe a linear resistance at low voltages caused by the decay of f_T (Fig. 7.3b), and a critical point (voltage) above which the resistance is equal to the normal state resistance. At higher temperatures ($T = 0.5\ T_c, 0.75\ T_c$) a linear approach would only give an adequate approximation in a limited voltage range. We will argue below that the superconductor switches to the normal state by f_L which is controlled by the *voltage* and cannot be interpreted as a critical current. In Fig. 7.5 the electrostatic potential $\phi = \int_0^\infty f_T\Re\{g\}d\epsilon$ along the wire is shown at zero temperature prior to ($eV/\Delta_0 = 0.013, 0.646$) and immediately after ($eV/\Delta_0 = 0.651$) the transition. The potential can be seen to drop to zero over a distance of the order of the coherence length due to the normal- to supercurrent conversion. This mechanism also gives rise to the finite zero bias resistance. The profile hardly changes
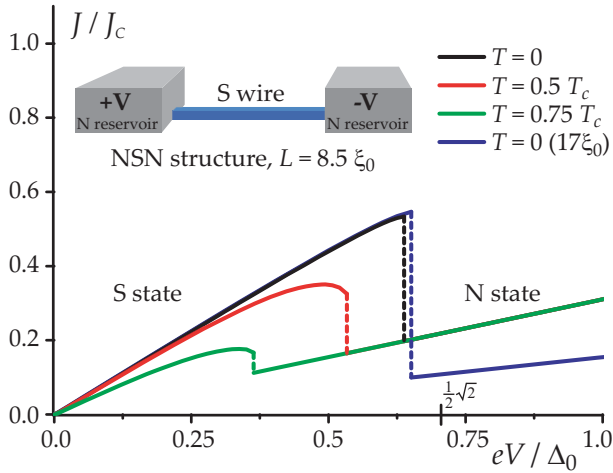
Figure 7.4: The calculated current(J)-voltage(V) relation of a superconducting wire of length $L = 8.5\xi_0$ between normal metallic reservoirs (see inset) at several temperatures, and for a wire of length $17\xi_0$ at $T = 0$. J_c is the critical current density, and Δ_0 the bulk gap energy.

over the full range of voltages, until the critical value is reached, after which the electrostatic potential drops in a linear fashion, indicating the system is in the normal state. The minimal changes emphasize the limited influence of f_T on the superconducting state (i.e. on Δ). The current density at which the
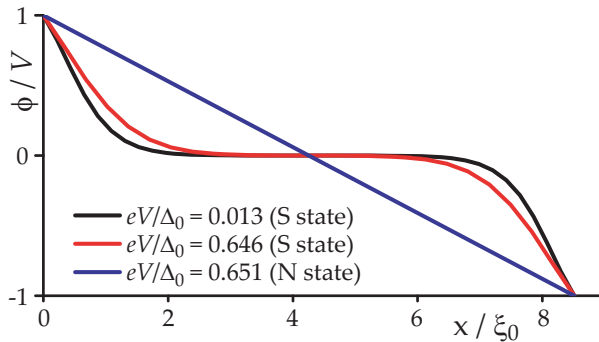

Figure 7.5: The normalized electrostatic potential ϕ as a function of position x along the superconducting wire for bias voltages prior to and immediately after the transition (at $T = 0$).

superconductor switches to the normal state (for $T = 0$) is much smaller than

the critical current density in an infinitely long wire ($J/J_c = 1$). This excludes the depairing mechanism as the (main) cause of the transition. Moreover, it is acceptable to ignore the occurrence of phase slip centers [87], which are time-dependent solutions that are energetically favorable when $J \approx J_c$. Neither is the transition triggered at the weaker superconducting edges as indicated by the shape of the electrostatic potential profile in Fig. 7.5.

7.1.4   Simulation on the non-local system

The parameter that determines whether or not the superconducting state exist is Δ, as follows from Eq. 7.13. The integral in this self-consistency equation sums all pair states (either occupied by a Cooper pair, or empty). F_i gives the Cooper pair density-of-states and f_L and f_T determine which of those states are doubly occupied or doubly empty and which are singly occupied (broken) due to the presence of quasiparticles. In equilibrium at $T = 0$, a switch to the normal state can only be caused by reaching a critical phase gradient, entering Δ via F_i. In the presence of quasiparticles, Δ (and thus potentially the state of the system) is also influenced by the distribution functions. It was noticed above that the charge mode f_T has a very limited influence on Δ. The effect of the energy mode f_L is examined below.

By a small modification of our system to a T-shaped geometry as shown in Fig. 7.6, we can in a direct way disentangle the effects of f_L and f_T on Δ. This setup can be thought of as the connection of the superconducting wire to the center of a normal wire. In the middle of such a wire f_T is equal to zero, but f_L is not. The result for the pair potential at the edge of the superconducting wire as a function of the voltage of the reservoirs is shown in Fig. 7.6. Although there is no net current flowing through the superconductor, at a certain voltage the pair potential collapses. The voltage that is necessary to trigger this transition to the normal state is very close to the transition in Fig. 7.4 (where we used the two terminal setup). Apparently the influence of f_L is important, since it can cause the superconductor to switch to the normal state irrespective of the value of the supercurrent. Clearly the influence of f_L on the state of the superconductor is larger than the influence of the supercurrent on this same quantity.

The quantity that defines the possible states of the system is the free energy. Evidently the superconductor compares two states for the minimization of this free energy: the first state is the superconducting state in which the free energy remains constant as a function of voltage (and independent of the shape of f_L provided this shape does not change for energies larger than the
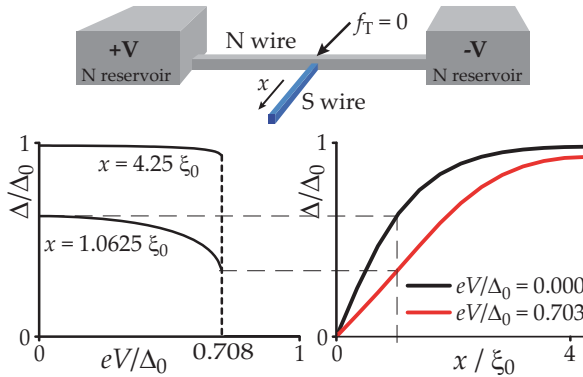
Figure 7.6: Top: T-shaped geometry, bottom: pair potential Δ in the S-wire as function of (left) voltage at two different positions; (right) position at two different voltages. The breakdown voltage is at $eV/\Delta_0 = 0.707$. The wire length is 4.25 ξ_0

gap). The second possible state is the normal state. At zero temperature, in the absence of a bias voltage, the difference in free energy between the two states is the condensation energy of the superconductor. When the voltage is increased (but still $eV < \Delta$), the free energy of the superconducting state remains constant while the free energy of the normal state decreases since in that case electrons occupy higher energy states due to the applied voltage. To illustrate the effect, we calculate explicitly the (internal) energy difference between the superconducting state (E_S) and normal state (E_N) at zero temperature for both a bulk superconductor (analytically) and the T-shaped structure (numerically) as a function of voltage (which appears in f_L) and Δ. From the analytical calculation for the bulk, following Bardeen [88], we find that f_L changes the energy in such a way that at $eV = \frac{1}{2}\sqrt{2}\Delta_0$ the superconductor undergoes a first order phase transition. For the voltage range $\frac{1}{2}\Delta_0 < eV < \Delta_0$ the state of the system has two solutions (two minima). The energy difference for the bulk superconductor is shown in Fig. 7.7. Numerical results for the energy of the T-shaped geometry are shown as well (both as function of position and as function of voltage). For long wires, the numerical results approach the analytical (bulk) calculation. This indicates that the effect of the bias voltage can indeed be related to the existence of a first order phase transition at zero temperature.

In conclusion, we have studied the role of the energy mode f_L of the quasi-

---

Hysteretic behavior due to the first order transition is also present in the numerical calculation, for clarity in Fig. 7.4 and 7.6 only the upsweeps are displayed.
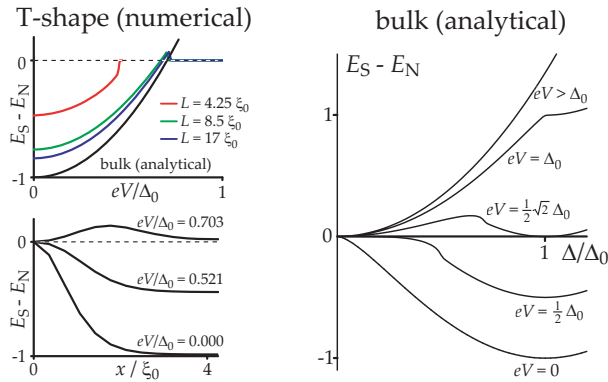
Figure 7.7: Energy difference between the superconducting and normal state. Right: analytical bulk solution showing the bistable voltage range. Left: numerical solutions for (top) increasing wire length as function of voltage and (bottom) for a $4.25\,\xi_0$ long wire as function of position (energy thus being a density). Energies are normalized to $\mathrm{H}_c^2(0)/8\pi$.

particle distribution on the properties of a superconducting nanowire. We employ a numerical simulation of the Usadel equation in full-response and find a non-thermal distribution for f_L (caused by an applied bias voltage) which drives a first order transition from the superconducting state to the normal state irrespective of the current. A direct calculation on the internal energy of a bulk superconductor confirms that the voltage indeed causes the phase transition. In general, the significant role played by f_L found in these superconducting nanowires stresses the importance of treating f_L and f_T on equal footing.